Elasticity and electrical resistivity of chalk and greensand during water flooding with selective ions

Katika, Konstantina; Alam, Mohammad Monzurul; Alexeev, Artem; Chakravarty, Krishna Hara; Fosbøl, P. L.; Revil, A.; Stenby, Erling Halfdan; Xiarchos, Ioannis; Yousefi, A.; Fabricius, Ida Lykke

Published in:
Journal of Petroleum Science and Engineering

Link to article, DOI:
10.1016/j.petrol.2017.11.045

Publication date:
2018

Document Version
Publisher's PDF, also known as Version of record

Journal of Petroleum Science and Engineering 161 (2018) 204–218

Contents lists available at ScienceDirect

Journal of Petroleum Science and Engineering

journal homepage: www.elsevier.com/locate/petrol

Elasticity and electrical resistivity of chalk and greensand during water flooding with selective ions

K. Katika [a], M.M. Alam [a], A. Alexeev [c], K.H. Chakravarty [c], P.L. Fosbøl [c], A. Revil [d], E. Stenby [b], I. Xiarchos [c], A. Yousefi [e], I.L. Fabricius [a,*]

[a] Department of Civil Engineering, Technical University of Denmark, Denmark
[b] Department of Chemistry, Technical University of Denmark, Denmark
[c] Department of Chemical Engineering, Technical University of Denmark, Denmark
[d] Université Savoie Mont-Blanc ISTERRE CNRS, France
[e] Politecnico di Torino, Italy

ARTICLE INFO

Keywords:
Water flooding with selective ions
Greensand
Chalk
Wettability
Fines formation
Pore compressibility

ABSTRACT

Water flooding with selective ions has in some cases lead to increased oil recovery. We investigate the physical processes on a pore scale that are responsible for changes in petrophysical and mechanical properties of four oil-bearing chalk and four oil-bearing greensand samples caused by flooding with brines containing varying amounts of dissolved NaCl, Na_2SO_4, $MgCl_2$ and $MgSO_4$. Ultrasonic P-wave velocity and AC resistivity measurements were performed prior to, during and after flow through experiments in order to identify and quantify the processes related to water flooding with selective ions. Low field Nuclear Magnetic Resonance (NMR) spectrometry measurements were performed at full water saturation, at irreducible water saturation, after aging and after flooding. CT-scanning, X-ray diffraction (XRD), backscatter electron microscopy images (BSEM), mercury injection capillary pressure (MICP) curves and specific surface analysis (BET) reveal the mineralogy and texture of the rock samples before and after the injection. Low field NMR data indicates changes in the pore fluid distribution and wettability of chalk after aging of one of the samples. NMR data for other samples indicate that chalk is water-wet after flooding. Greensand remained mixed wet throughout the experiments. Electrical resistivity data are in agreement with this interpretation. The electrical resistivity data during flooding revealed that the formation brine is not fully replaced by the injected water in both chalk and greensand. Changes in the elasticity of chalk during flooding illustrate the softening effect of magnesium bearing brines as compared to the sodium bearing brines. The stiffness of greensand was not affected by water flooding with selective ions as determined from the elastic wave measurements. Precipitation of fines during flooding of chalk samples is indicated by an increase in specific surface area and a shift in the MICP to lower values but no fines were detected by NMR. No changes were observed for greensand samples.

1. Introduction

Waterflooding with selective ions can enhance the production of oil from reservoirs (Morrow et al., 1998; Seccombe et al., 2008). Previous studies, both in the field and in the laboratory, have validated the success of this class of procedures to increase oil production both from carbonate and siliciclastic reservoirs. Low salinity flooding has been successfully used in sandstone reservoirs (Seccombe et al., 2008; Vledder et al., 2010) and effects of changing the composition of the injecting water have been observed in limestones (Morrow et al., 1998; Strand et al., 2006; Austad et al., 2008). That said, the mechanisms by which oil production can be enhanced are not clear (Jackson et al., 2016; Yutkin et al., 2016), so we will by petrophysical monitoring of flooding experiments address three possible mechanisms related to waterflooding with selective ions: 1) the wettability alterations of chalk and greensand during aging and waterflooding; 2) the changes in the elastic properties of the rock due to solid/fluid interactions; 3) the generation of fines and precipitation or other substitution/adsorption phenomena on the pore wall of the rock due to the injection of water with various ions.

Wettability describes the solid-fluid affinity of a unique system of brine, oil and rock under certain conditions; such as temperature and pressure (Radke et al., 1992). By systematically varying wettability of

* Corresponding author.
E-mail address: ilfa@byg.dtu.dk (I.L. Fabricius).

https://doi.org/10.1016/j.petrol.2017.11.045
Received 15 March 2017; Received in revised form 26 October 2017; Accepted 17 November 2017
Available online 21 November 2017

Berea sandstone, Jadhunandan and Morrow (1995) showed an optimum in oil recovery by water flooding when the rock is water wet before the water injection. Several studies also report that increased flooding efficiency in chalk can be caused by alteration towards water wetness, due to the sorption of surface-potential-determining divalent ions (Austad et al., 2005, 2008; Strand et al., 2006; Puntervold and Austad, 2008; Yousef et al., 2011). In this context Hiorth et al. (2010) modelled mineral dissolution of chalk due to the injection of water containing divalent ions and discussed the effect of this dissolution upon the wettability of the chalk. We will use low field NMR and electrical resistivity to discuss sample wettability because the NMR signal from a fluid depends on the direct interaction with the mineral surface (Guan et al., 2002; Al-Mahrooqi et al., 2003); and because electrical resistivity of a saturated rock increases by alteration from water-wet to oil-wet (Sweeney and Jennings, 1960), so that we expect an increase in the n-saturation exponent from Archie's law.

A weakening of chalk when water or brines are introduced into the pore space was already noticed by Newman (1983) and is referred to as water weakening. Also stiffness is affected by pore fluid, and Katika et al. (2015) observed that chalks from Stevns Klint saturated with high salinity Mg-rich brines, are softer than chalks saturated with Na-rich brines. Korsnes et al. (2006) suggested that water weakening of chalk due to injection of seawater-like brines is related to substitution of Ca^{2+} ions with Mg^{2+} at the grain-to-grain contacts in the presence of SO_4^{2-}. On the other hand, experiments on Stevns and Leige chalk by Madland et al. (2011) demonstrated that sulphate is not needed to have a significant amount of deformation, although lower concentration of magnesium ions were found in the produced than the injected pore water. Two mechanisms were proposed; substitution of calcium and magnesium without the presence of sulphates in the pore water and the precipitation of magnesium as part of a new mineral phase (Madland et al., 2011; Andersen et al., 2012). Nermoen et al. (2015) observed the effect of various brines and oil on the elastic properties of Liege chalk from Belgium, as derived from mechanical testing. The proposed mechanism is that chalk saturated with brines which cause high electrostatic potential on the surface of chalk, are the weakest. Nermoen et al. (2015) introduced the repulsive electrostatic stress as a mechanism that separates the grains of chalk and therefore weakens the saturated sample.

Changing pore water composition can lead to precipitation of minerals onto the surface of solids in the rock or to precipitation of fines (Fathi et al., 2010; Madland et al., 2011; Yousef et al., 2011). In the above-mentioned study, Hiorth et al. (2010) proposed that a precipitation/dissolution mechanism can be the controlling factor that influences the oil recovery of carbonate rocks as observed in laboratory experiments in previous studies (Zhang et al., 2007; Austad et al., 2008).

2. Rock materials and brines

2.1. Reservoir chalk from the Gorm field

Chalk is a sedimentary carbonate rock of high homogeneity, but its petrophysical properties fall in wide ranges. Porosity and specific surface are main determining factors for permeability and capillary entry pressure, and partly for elastic moduli (e. g. Fabricius, 2007). The selected reservoir chalks of Tor Formation are from the Gorm (N-3X) field in the North Sea (Bæk, 2014). Five horizontal or vertical plugs (75 mm length and 37 mm diameter) were used for aging and flooding experiments and side and end trims were selected for the petrophysical investigation.

2.2. Reservoir greensand from Solsort field

The aged and flooded greensand is a mixture of quartz grains and chlorite aggregates from the Solsort field (Bæk, 2014) in the North Sea. The mineral responsible for the microporosity of the greensand is chlorite which is known for a high paramagnetic index (Hürlimann et al., 2004) and high stiffness (Wang et al., 2001). Five horizontal core plugs, of 50 mm length and 37 mm diameter, were used for aging and flooding experiments and side and end trims were selected for the petrophysical investigation.

Table 1
Composition of the Formation waters for the two reservoirs from which the cores were extracted.

Parameter	Gorm field (Chalk reservoir)	Solsort field (Greensand reservoir)
Na^+ (mg/L)	13500	11300
K^+ (mg/L)	100	360
Mg^{2+} (mg/L)	95	23
Ca^{2+} (mg/L)	250	105
Cl^- (mg/L)	21000	18225

Table 2
Dan field dead oil properties.

Dead oil	Mass density (g/cm^3)	Acid number (mg KOH/g oil)	Base number (mg KOH/g oil)	Asphaltene (%)	Viscosity (cp)
Dan Field	0.845	0.09	2.44	0.3	8.83

2.3. Brines and oil

The composition of the formation water for each field is given in Table 1, but for the sake of fluid compatibility, all plugs were saturated with brine corresponding to Dan field Brine and dead oil from the Dan field (Bæk, 2014) in North Sea (Table 2). Two sets of brines were used in the core flooding experiments; Na-bearing and Mg-bearing (Table 3). The resistivity of the injected brines were calculated from SLB chart 9 (Schlumberger, 2000).

The produced fluids were collected in effluent tubes during the flow through experiments. The amount of produced oil in each tube was measured by image analysis and by using the liquid scintillation method (Katika et al., 2016).

Table 3
Compositions of brines used for core flooding.

Na brines mol/kg H_2O	NaCl	Na_2SO_4	Mg brines mol/kg H_2O	$MgCl_2$	$MgSO_4$
0.6 Cl^-	0.6	–	0.6 Cl^-	0.3	–
0.3 SO_4^{2-}	–	0.3	0.3 SO_4^{2-}	–	0.3
0.3 Cl^- + 0.15 SO_4^{2-}	0.3	0.15	0.3 Cl^- + 0.15 SO_4^{2-}	0.15	0.15
0.6 Cl^- + 0.75 SO_4^{2-}	0.6	0.75	0.6 Cl^- + 0.75 SO_4^{2-}	0.3	0.375
0.06 Cl^-	0.06	–	0.06 Cl^-	0.03	–

Table 4
Water and oil saturation of chalk from the Gorm field and greensand from the Solsort field before aging and water flooding at 60 °C (N-3X X02H and D08H were not flooded).

Sample ID	Water saturation, %	Oil saturation, %
N-3X 04H	5	95
N-3X 09H	13	87
N-3X 11H	12	88
N-3X 17V	13	87
N-3X X02H	5	95
D03H	46	54
D04H	33	67
D07H	38	62
D17H	34	66
D08H	44	56

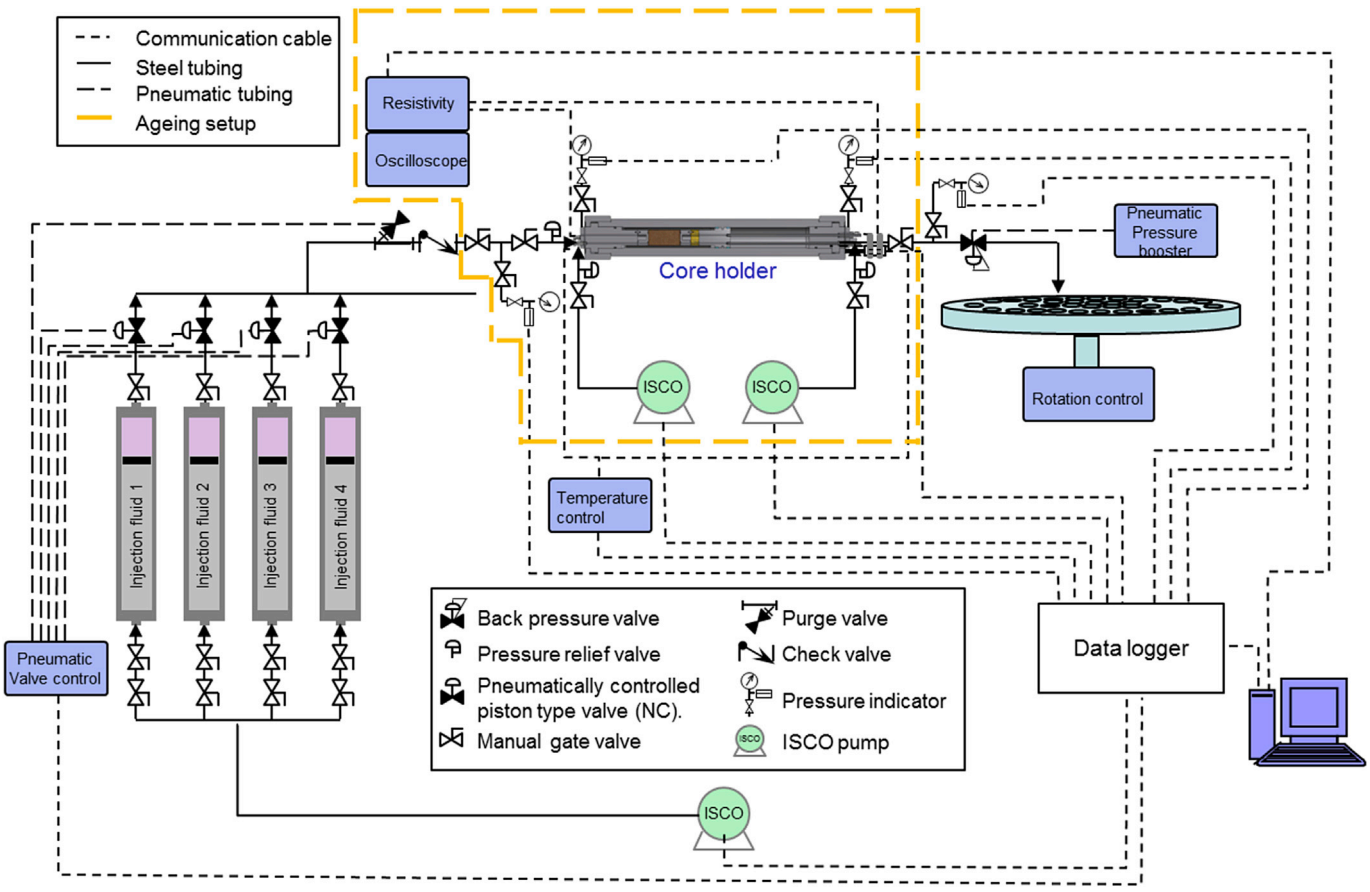

Fig. 1. Sketch of the core flooding setup.

3. Methods

3.1. Rock characterization

The petrophysical properties of chalk and greensand core samples were determined in dry and saturated conditions and thereafter in both aged and flooded conditions. The plugs were first cleaned for salt and hydrocarbons using the Soxhlet extraction method: refluxed by methanol to remove salts and toluene to remove the hydrocarbons (API, 1998). Clean samples were then dried in an oven for two days, at a temperature of 55 °C in order to avoid potential damage to clay minerals. In dry conditions the grain density, porosity and Klinkenberg corrected permeability were determined using a PoroPerm Production 2 gas porosimeter from Vinci Technologies. The core plugs were CT-scanned to ensure their homogeneity before aging and flooding. Side trims from the same cores were used for the determination of mineralogy by X-ray diffraction (XRD) and the specific surface. The specific surface area (S_{BET}) (m^2/g) was obtained with the nitrogen adsorption method using the technique proposed by Brunauer, Emmet and Teller (BET) (Brunauer et al., 1938). The BET measurements were performed, using the Autosorb iQ gas sorption system from Quantachrome Instruments. Backscatter electron microscopy (BSEM) photos were obtained from polished thin sections. The pore throat size distribution of the dry rocks was determined by mercury porosimetry (MICP) utilizing a Poremaster® PM 33-GT-12 analyzer.

Ultrasonic velocities V_P and V_S were acquired at 2 MPa unconfined stress to define the elasticity of the samples at dry conditions. Later, all core plugs were fully saturated with water and low field NMR spectrometry, V_P, V_S and electrical resistivity measurements were performed in water saturated conditions. Using a predetermined method (flushing for greensand and evaporation for chalk), the core plugs reached their irreducible water saturated state and the rest of the pore space was occupied with dead oil from the North Sea (Dan field) (Katika et al., 2017) (Table 4). Thereafter, the core plugs were examined by NMR spectrometry and CT-scanning. All samples were aged and flooded at 60 °C.

Table 5
Bulk and shear moduli of the fluids and minerals of the core plugs.

Rock	K (GPa)	G (GPa)	Citation
Calcite	70	29	Mavko et al., 2009
Quartz	36	45	Mavko et al., 2009
Chlorite	164	51	Wang et al., 2001
Dan field formation water	2.32	–	Batzle and Wang, 1992
Solsort field formation water	2.29	–	Batzle and Wang, 1992
Crude oil Dan field	1.61	–	Batzle and Wang, 1992

3.2. Aging and waterflooding setup

A high temperature-high pressure core flooding apparatus was utilized for the flow through experiments. The core flooding system consists of a Hassler type core holder to hold an 1.5 inch diameter core plug, two pumps controlling the axial and radial stress applied on the core and a heat jacket to maintain the temperature at 60 °C during aging and flooding. A back pressure regulator maintains the pore pressure, a pneumatic valve regulates the flow from the four cylinders injecting the brine or water in the core plug and an additional pump is connected to the cylinders to assist the fluid injection. All brines were injected in the cores at a flow rate of 0.1 ml/min. An oscilloscope is connected to the pistons in touch with the core plug, in order to determine the changes in the travel time of the elastic waves throughout the flow through experiments. A variable resistor is connected in series with the core plug in a

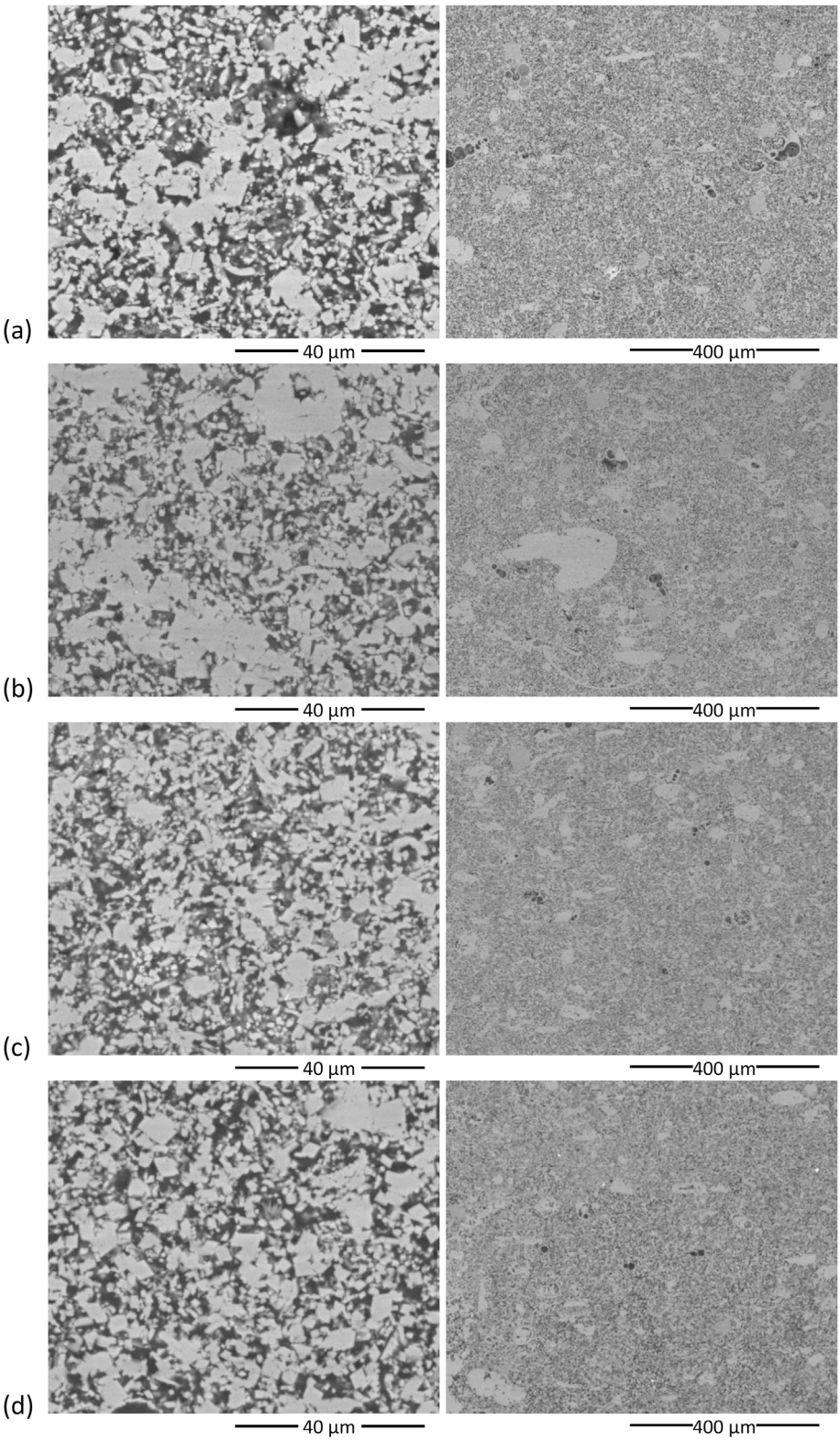

Fig. 2. BSEM image in high (left) and low (right) resolution for the chalk samples from the Gorm field well; (a): N-3X 04H (6877 ft-md), (b): N-3X 09H (6901 ft-md), (c): N-3X 11H (6915 ft-md), and (d): N-3X 17V (7033 ft-md). All images recorded with a Quanta 200 (FEI) scanning electron microscope on polished thin sections of the end trims of the core plugs.

1 kHz AC circuit of 1 volt power supply to determine the electrical resistance, which then is converted into resistivity using a geometrical factor. After the back-pressure regulator, effluents (fluids exiting the core during flooding) are channelled into the fraction collector. The core flooding setup is shown in Fig. 1.

3.3. Monitoring by ultrasonic waves

After the saturation with water and oil at irreducible water saturation, the core plugs were sealed in the core holder for aging and later flooding (Fig. 1). During aging and waterflooding, elastic wave velocity and

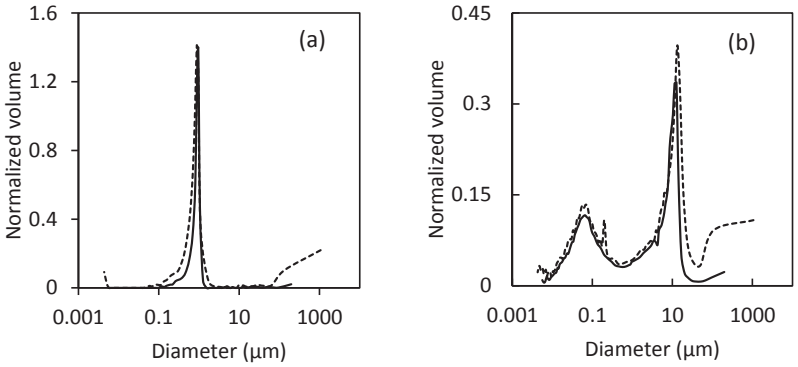

Fig. 3. Throat size distribution from MICP for (a) the chalk from Gorm field (sample N-3X 09H), and (b) chloritic greensand from Solsort field (sample D07H). The solid line represents the throat diameter before flooding, and the dashed line is after flooding and cleaning (Poremaster® PM 33-GT-12, mercury porosimetry analyzer).

Table 6
Mineral composition of the studied material (-M- representing the major components and -m- the minor components). Samples were analyzed by X-ray diffraction (XRD) by using Cu K-α radiation with a Philips PW 1830 diffractometer.

Mineral	Gorm field Chalk	Solsort field Greensand
Quartz	m	M
K-Feldspar	m	traces
Calcite	M	traces
Kaolinite	m	m
Chlorite	m	M
Illite	–	m
Smectite	–	–

electrical resistance data were continuously recorded every 15 min.

In order to evaluate the stiffness of the rock we calculated the elastic moduli from ultrasonic wave velocities. The compressional wave modulus, M (GPa), is related to the compressional wave velocity, V_P (km/s), and the density, ρ (g/cm^3). The shear wave modulus, G (GPa), is related to the shear wave velocity, V_S (km/s), and the density. The two moduli provide information about the bulk modulus, K (GPa), of the rock as shown in the following equations:

$$M = \rho V_P^2 \quad (1)$$

$$G = \rho V_S^2 \quad (2)$$

$$K = \rho V_P^2 - \frac{4}{3}\rho V_S^2. \quad (3)$$

The drained bulk modulus, K_f (GPa) was modelled by Gassmann's fluid substitution, for all the fluid saturated rocks (Gassmann, 1951):

$$\frac{K_{sat}}{K_m - K_{sat}} = \frac{K_f}{K_m - K_f} + \frac{K_{fl}}{\phi(K_m - K_{fl})} \quad (4)$$

where K_{sat} (GPa) is the bulk modulus for the saturated rock, ϕ is the porosity, K_m (GPa) is the mineral bulk modulus and K_{fl} (GPa) is the modulus of the saturating fluid. The bulk moduli of the fluids were

Table 8
V_P and V_S of chalk from the Gorm field at 2 MPa axial unconfined stress and room temperature (dry conditions).

Sample ID	V_{Pdry} (km/s)	V_{Sdry} (km/s)
Error	±0.05	±0.1
N-3X 04H	2.22	1.38
N-3X 09H	2.53	1.52
N-3X 11H	2.64	1.64
N-3X 17V	2.74	1.74
N-3X X02H	2.20	1.58

determined from Batzle and Wang (1992). The modulus of each mineral and fluid used in our calculation are given in Table 5. The pore compressibility, $\frac{1}{K_\phi}\left(\frac{1}{GPa}\right)$, was determined from the frame and mineral moduli:

$$\frac{1}{K_\phi} = \frac{K_m - K_f}{K_f K_m \phi}, \quad (5)$$

or Biot's coefficient, β (Mavko et al., 2009):

$$\frac{1}{K_\phi} = \frac{\beta}{K_f \phi}. \quad (6)$$

3.4. Monitoring by electrical resistivity

For evaluation of hydrocarbon reservoirs, electrical resistivity is typically used in calculating hydrocarbon saturation when knowing saturation exponent, pore water resistivity and porosity. In the present study, porosity, hydrocarbon saturation and initial pore water resistivity are known already. During aging we can then monitor the saturation exponent, and during flooding, we can calculate the net pore water resistivity and thus estimate the efficiency of water replacement. Based on the measured electrical resistance during aging, and the fluid saturation of the rock at a given state, the n-saturation exponent can thus be determined by Archie's equation (Archie, 1942), provided we may neglect the contribution from surface conductivity:

Table 7
Petrophysical properties of chalk from the Gorm field (N-3X X02H was not flooded).

Sample	Grain density (g/cm^3)	Porosity (%)	Klinkenberg Permeability (mD)	BET (m^2/g)	Carbonate Content (wt%)
Error	±0.01	±0.3	±0.1	±0.03	±0.5
N-3X 04H	2.71	39.9	4.8	1.4	98
N-3X 09H	2.67	35.3	3.6	1.5	95
N-3X 11H	2.67	36	4.1	1.3	97
N-3X 17V	2.68	34.1	3.8	0.9	97
N-3X X02H	2.71	37.5	4.1	1.3	98

Table 9
V_P and V_S and electrical resistivity of chalk from the Gorm field at 2 MPa axial unconfined stress at room temperature (full formation water saturated conditions).

Sample ID	Water saturation, %	V_{Pwet} (km/s)	V_{Swet} (km/s)	Electrical resistivity (Ohm-m)	m
Error	±1	±0.05	±0.1	±0.1	
N-3X 04H	99	2.35	1.08	4.5	1.45
N-3X 09H	100	2.53	1.22	5.9	1.55
N-3X 11H	100	2.69	1.07	7.7	1.81
N-3X 17V	100	2.99	1.07	7.7	1.72
N-3X X02H	99	2.23	1.35	5.6	1.60

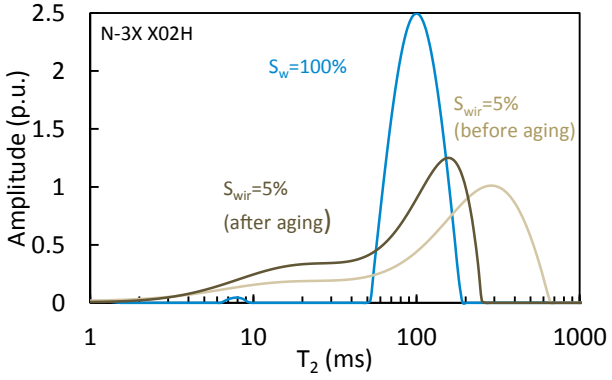

Fig. 4. The T_2 distribution of a chalk sample from the Gorm field (N-3X X02H) at full water saturation conditions (S_w); at full water and oil saturation at irreducible water saturation, before and after aging (S_{wir}) (N-3X X02H was not flooded). All measurements performed at ambient temperature and pressure using an Oxford Instruments GeoSpec 2/53 DRX-HF digital spectrometer. The nominal frequency of the magnet is 2 MHz. A CPMG pulse sequence was used with 32768 echoes (NECH), 32 scans (NS) and CPMG inter echo spacing (τ) 200 μs.

$$S_w^n = \left(\frac{R_w}{\phi^m * R_t}\right) \quad (7)$$

where:

R_w = Saturating brine resistivity calculated from the composition of the brines (Tables 1 and 3) (Schlumberger, 2000) (Ohm m)
ϕ = Porosity
m = Cementation exponent
R_t = Resistivity of partially saturated rock (Ohm m).

A contribution from surface conductivity to R_o need not be taken into account in this case, because the relatively high conductivity of formation water ($\sigma_w > 0.01$ Sm^{-1}) makes this effect negligible (Revil, 2013a, b).

The cementation exponent for each sample was determined individually from the formation factor, where R_0 (Ohm m), is the resistivity of the fully water saturated sample:

$$F = \frac{R_0}{R_w} = \frac{1}{\phi^m} \quad (8)$$

During flooding, using the n-saturation exponent determined from aging for each sample, we determined the resistivity of the saturating brine, R_w (Ohm m), and compared it with the injection fluids. This way, we are able to determine whether the injecting brine is able to displace all the formation brine.

4. Results

4.1. Petrophysical investigation before flooding

4.1.1. Chalk from Gorm field

The chalk samples from the Gorm field have a bimodal grain size distribution (Fig. 2), but the pore size distribution is unimodal and narrow as observed from the MICP curve in Fig. 3. The results from the XRD analysis are shown in Table 6 indicating the dominance of calcite but presence of silicates. The petrophysical properties of the core plugs; including grain density, porosity, permeability, carbonate content, and BET specific surface area, are shown in Table 7. Table 7 includes an

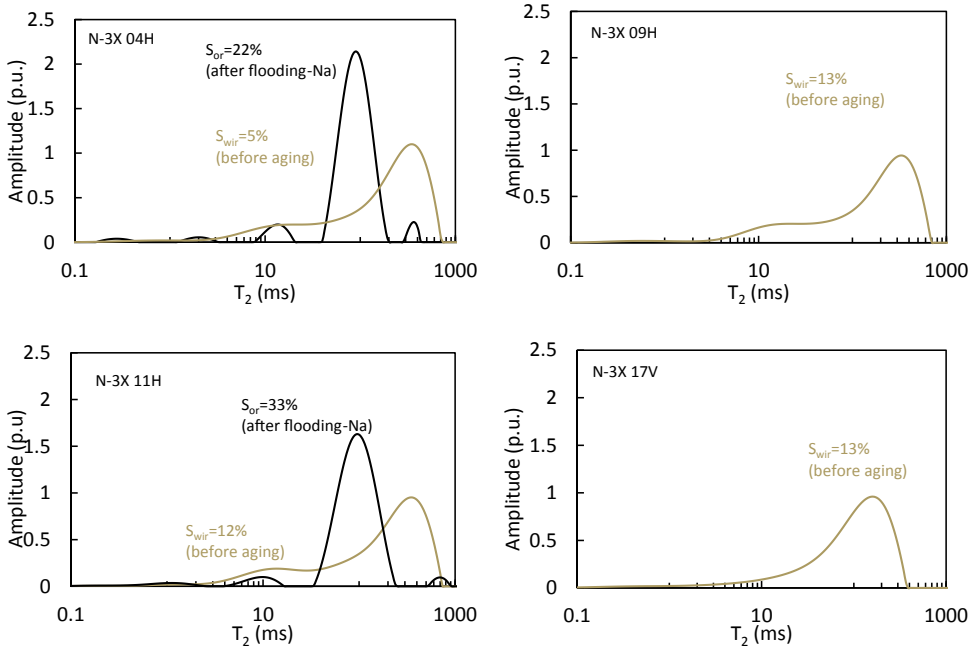

Fig. 5. The T_2 distributions of the water flooded chalk samples from the Gorm field (N-3X 04H, N-3X 09H, N-3X 11H, N-3X 17V) at full water and oil saturation at irreducible water saturation (S_{wir}), and after water flooding (S_{or}). All measurements were performed at ambient temperature and pressure.

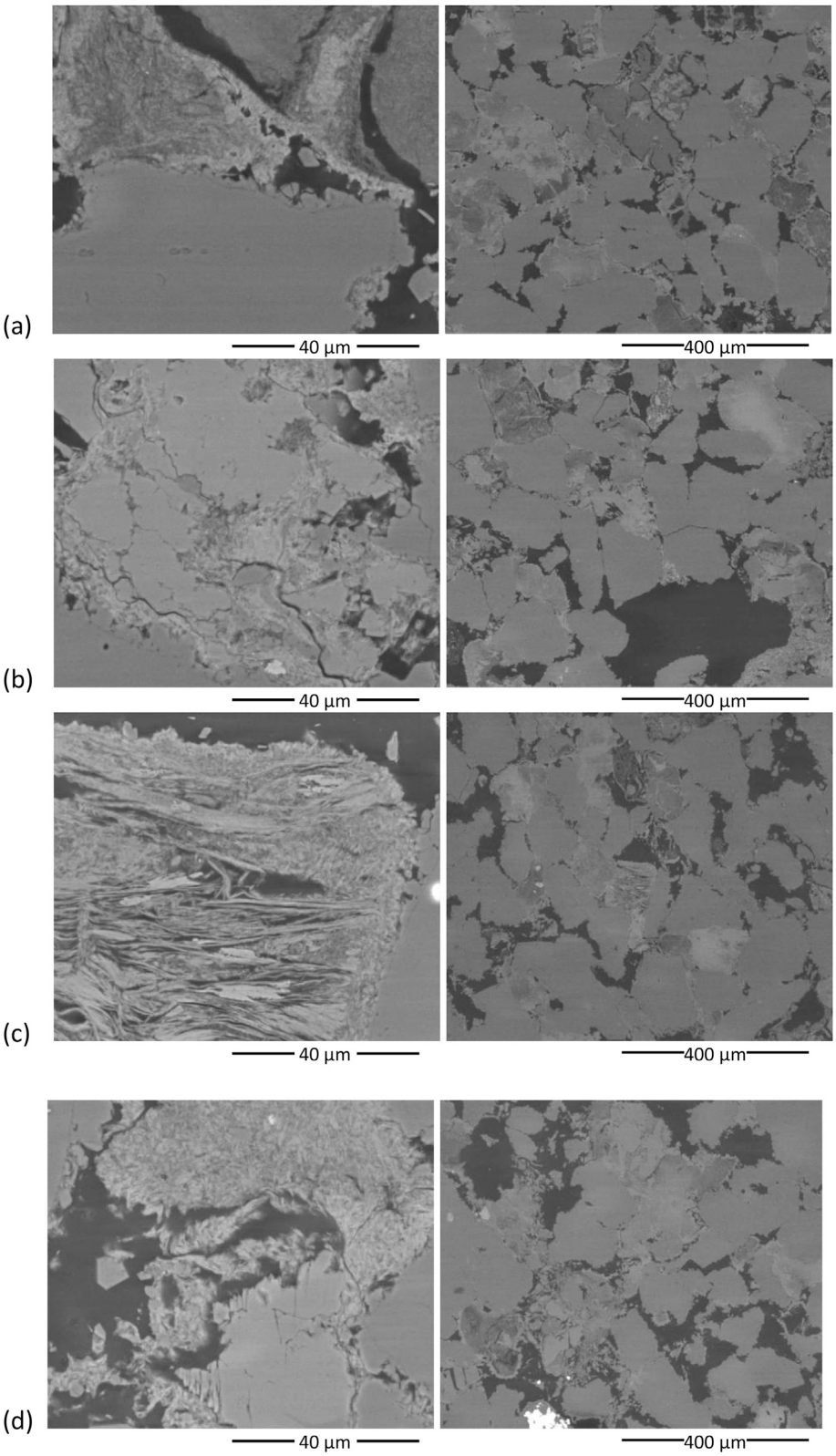

Fig. 6. BSEM image in high (left) and low (right) resolution for the greensand samples from the Solsort field well; (a): D03H (3702 ft-md), (b): D04H (3012 ft-md), (c): D07H (3706 ft-md), and (d): D17H (3716 ft-md). All images recorded with a Quanta 200 (FEI) scanning electron microscope on polished thin sections of the end trims of selected core plugs.

additional sample (N-3X X02H) that was saturated and aged, but not flooded. This core is the only chalk sample where we obtained the NMR spectrum directly after aging. The V_P and V_S of the dry chalk samples at 2 MPa are shown in Table 8, and data for the formation water saturated samples (velocities, electrical resistivity and cementation exponent at 2 MPa and room temperature) are shown in Table 9. The cementation exponent was determined for each sample individually from equation (7) at fully water saturated conditions.

Low field NMR spectrometry provides the T_2 distributions of the chalk in fully water saturated condition, where a single peak illustrates

Table 10
Petrophysical properties of greensand from the Solsort field (D08H was not flooded).

Sample ID	Grain density (g/cm^3)	Porosity (%)	Gas Permeability (mD)	BET (m^2/g)
Error	±0.01	±0.3	±0.1	±0.03
D03H	2.72	30	94	8.0
D04H	2.74	32	156	7.4
D07H	2.72	33	130	7.4
D17H	2.73	32	74	6.8
D08H	2.75	29	57	7.3

Table 11
V_P and V_S of greensand from the Solsort field at 2 MPa unconfined axial stress and room temperature (dry conditions).

Sample ID	V_{Pdry} (km/s)	V_{Sdry} (km/s)
Error	±0.05	±0.1
D03H	2.27	1.29
D04H	2.28	1.17
D07H	2.25	1.16
D17H	2.30	1.21
D08H	2.43	1.36

the homogeneous pore space (Fig. 4). The T_2 distributions of most chalk samples at oil and water saturation, demonstrate two distinct peaks; one between 10 and 20 ms for the water bound to the surface and another peak at 300 ms representing the relaxation of the oil present in the pore space as a practically free fluid (Figs. 4 and 5). The T_2 distribution of a single chalk sample (N-3X 17V) shows only one peak. The absence of a distinct water peak and the relatively low T_2 (140 ms) indicate that both oil and water contact the surface of the mineral.

4.1.2. Greensand from Solsort field

Backscatter electron micrographs and XRD analysis show that the greensand samples are containing quartz grains and chlorite aggregates (Fig. 6, Table 6) and a bimodal pore size distribution is shown from MICP (Fig. 3). The petrophysical properties of the core plugs (including grain density, porosity, permeability and BET specific surface area) are shown in Table 10. This table includes an additional sample (D08H) that was saturated with water and oil and aged, but not flooded, so that a T_2 distribution after aging could be obtained. The rest of the greensand samples were waterflooded directly after aging. The V_P and V_S of the dry greensand samples at 2 MPa are provided in Table 11, and data derived after saturation with formation water (velocities and electrical resistivity at 2 MPa and room temperature) are provided in Table 12.

The NMR T_2 distribution of the greensand samples from the Solsort field in fully water saturated conditions implies a bimodal pore size distribution (Figs. 7 and 8). The fast relaxing components of the T_2 distribution of all greensand samples at full water saturation (S_w) and at oil and water saturation (S_{wir}) are similar for all saturations (Figs. 7 and 8). This is an indication that in both cases water occupies the small pores of the rock.

Table 12
V_P and V_S and electrical resistivity of greensand from the Solsort field at 2 MPa unconfined axial stress at room temperature (formation water saturated conditions).

Sample ID	Water saturation, %	V_{Pwet} (km/s)	V_{S1wet} (km/s)	Electrical resistivity (Ohm-m)	m
Error	±1	±0.05	±0.1	±0.1	
D03H	93	2.58	1.30	2.9	2.12
D04H	94	2.61	1.32	2.5	2.08
D07H	100	2.59	1.30	2.5	2.13
D17H	99	2.58	1.29	3.1	2.28
D08H	96	2.71	1.36	3.1	2.09

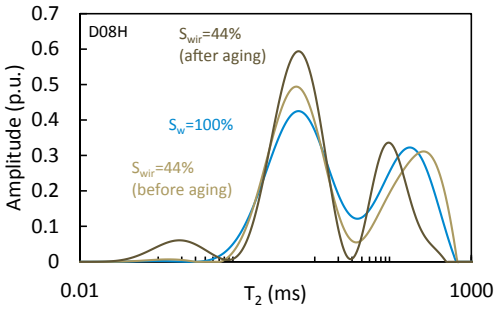

Fig. 7. The T_2 distribution of a greensand sample from the Solsort field (D08H) at full water saturation conditions (S_w); at full water and oil saturation at irreducible water saturation, before and after aging (S_{wir}) (D08H was not flooded). All measurements were performed at ambient temperature and pressure.

4.2. Aging at S_{wir}

During aging, the pore compressibility (1/Kϕ) for all samples was determined from ultrasonic data by Gassmann's fluid substitution. The pore compressibility was also determined from the compressional modulus and compared to the inverse shear modulus. The average values are presented in Table 13. The n-saturation exponent was determined from Archie's equation during aging neglecting the effect of surface conductivity. The stabilization of the exponent signifies the end of aging. The final value of n was later used to predict the brine resistivity during flooding. NMR T_2 distributions obtained after aging are shown in Fig. 4 (chalk) and Fig. 7 (greensand).

4.2.1. Chalk from Gorm field

Core plugs N-3X 04H, N-3X 09H, N-3X 11H and N-3X 17V were aged at 10 MPa axial and radial stresses and 60 °C. Time zero (t = 0 d) in all graphs is considered the moment at which the core plug was sealed inside the coreholder for aging. Fig. 9 shows the evolution of the pore compressibility, 1/Kϕ (1/GPa), from ultrasonic data, modelled from Gassmann's fluid substitution of chalk during aging and Fig. 10 shows the evolution of the n-exponent at same conditions.

During aging of chalk samples N-3X 09H, N-3X 11H and N-3X 17V, the pore compressibility varies between 0.15 and 0.25 (1/GPa), whereas for the case of N-3X 04H, the high pore compressibility, suggests the presence of fractures in the pore space (Fig. 9).

During aging of chalk samples N-3X 09H and N-3X 11H, the saturation exponent n varied between n = 2 and n = 3 indicating strongly water-wet conditions (Fig. 10). The n-saturation exponent of sample N-3X 04H during aging is lower than $n = 2$ probably due to the presence of fractures in the core plug. On the other hand, chalk sample N-3X 17V demonstrates a high n-saturation exponent, which may be the outcome of intermediate oil wetness (Suman and Knight, 1997) already pesent before aging as indicated by NMR (Fig. 5). A change in wettability is indicated by NMR data for sample N-3X X02H, because the oil peak at the long relaxing components of the T_2 distributions relaxes faster than before aging; the relaxation of the water peak (bound water) remains the same in both cases (Fig. 4).

4.2.2. Greensand from Solsort field

Core plugs D03H, D04H, D07H and D17H were aged at 10 MPa (axial and radial) stress. Time zero (t = 0 d) in all graphs is considered the moment the core plugs were sealed inside the core holder for the aging. Fig. 11 shows the pore compressibility, 1/Kϕ (GPa), from ultrasonic data, modelled from Gassmann's fluid substitution of greensand during aging and Fig. 12 shows the n-exponent at same conditions.

During aging of greensand samples, the n-saturation exponent varies between n = 3 and n = 4. The higher exponent of greensand compared to chalk may be the result of the mixed wettability of greensand (Katika

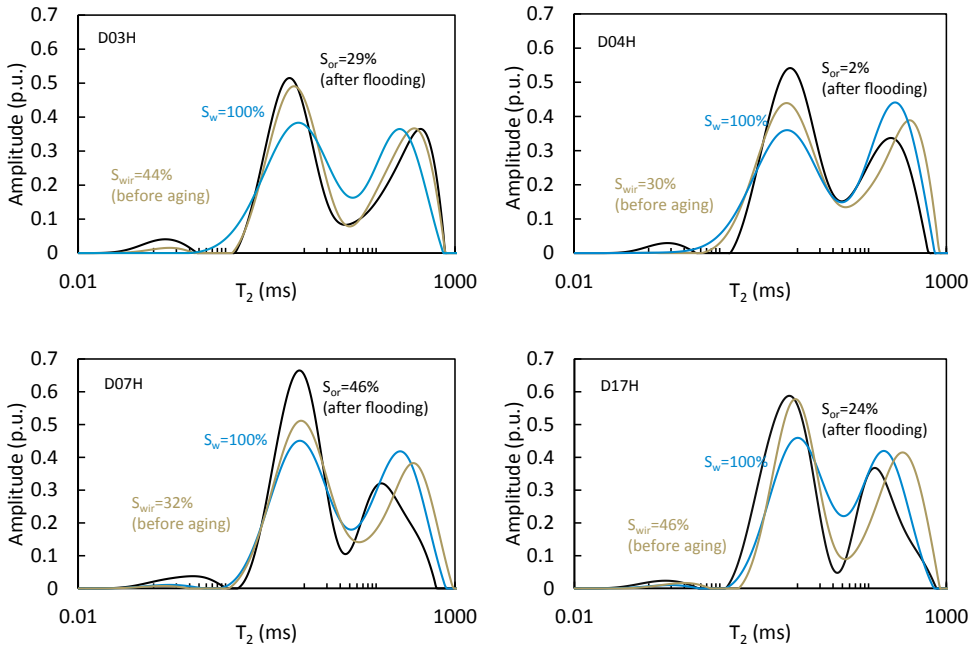

Fig. 8. The T_2 distribution of the water flooded greensand samples from the Solsort field (D03H, D04H, D07H and D17H) at full water saturation conditions (S_w); at full water and oil saturation at irreducible water saturation (S_{wir}), and after water flooding (S_{or}). All measurements were performed at ambient temperature and pressure.

Table 13
The average pore compressibility for all the samples, determined at dry and fully water saturated conditions, as well as during aging and flooding.

Sample ID	Lithology	Campaign	Average pore compressibility (1/GPa)											
			Dry conditions			Full water conditions			During aging			During water flooding		
			1/Kϕ	1/Mϕ	1/Gϕ	1/Kϕ	1/Mϕ	1/Gϕ	1/Kϕ	1/Mϕ	1/Gϕ	1/Kϕ	1/Mϕ	1/Gϕ
N-3X 04H	Chalk from Gorm field	Na	0.45	0.23	0.65	0.53	0.1	0.97	0.6	0.1	0.7	0.24	0.15	0.57
N-3X 09H		Mg	0.38	0.2	0.54	0.43	0.34	0.8	0.19	0.15	0.53	0.18	0.14	0.54
N-3X 11H		Na	0.37	0.18	0.47	0.31	0.05	0.54	0.25	0.05	0.54	0.24	0.18	0.56
N-3X 17V		Mg	0.38	0.18	0.44	0.18	0.17	1.13	0.18	0.15	0.65	0.21	0.15	0.49
D03H	Greensand from Solsort field	Na	0.58	0.31	0.91	0.16	0.04	0.68	0.20	0.04	0.45	0.18	0.05	0.52
D04H		Mg	0.44	0.28	1.01	0.18	0.04	0.48	0.20	0.04	0.43	0.19	0.04	0.43
D07H		Na	0.5	0.3	1.02	0.09	0.03	0.67	0.11	0.03	0.40	0.12	0.03	0.39
D17H		Mg	0.42	0.26	0.94	0.22	0.05	0.66	0.21	0.05	0.65	0.18	0.04	0.52

et al., 2017). A mixed wettability after aging is also indicated by NMR data: After aging the greensand sample D08H the oil peak at the long relaxing components of the T_2 distributions relaxes faster similarly to the chalk sample N-3X X02H. The water peak (bound water) remains the same in both cases (Figs. 7, 8).

4.3. Water flooding with selective ions

The pore compressibility (1/Kϕ) from ultrasonic data, was modelled from Gassmann's fluid substitution during flooding of all samples. The bulk density was calculated based on the dry density of the samples, the oil recovery, the fluid injection and effluent analysis.

The n-saturation exponent determined from Archie's equation during aging at 60 °C for each sample was used to predict the resistivity of the brine in the pore space of the rock during flooding at 60 °C (equation (7)). Assuming that the injected brine might bypass part of the formation brine, then the resistivity measurements during flooding is a good indicator of the amount of fluid in the pore space that was not replaced.

4.3.1. Chalk from Gorm field

Core plugs N-3X 17V, N-3X 11H, N-3X 09H and N-3X 04H were flooded at 39 MPa axial and 40 MPa radial stress at 60 °C. Fig. 13 shows the pore compressibility from ultrasonic data during flooding and the oil recovery curve, and Fig. 14 shows the resistivity of the injected brine, the resistivity of the brine present in the pore space during water flooding as well as the resistivity of the core plug at the same conditions.

During flooding of chalk, when the radial and axial stresses rise, the pore compressibility of the possibly fractured sample N-3X 04H resumes to lower values similar to the other chalk samples (Fig. 13). This is in accordance with the rising electrical resistivity that demonstrates the closure of cracks and fractures after the application of high axial and radial stresses (Fig. 14).

During flooding of the chalk samples, the resistivity of the pore water remains higher than the resistivity of the injected brine (Fig. 14). This indicates that the water injection did not fully replace the formation brine present in the pore space of each sample so that the water flow during injection bypassed parts of the pore space. The bypass of parts of the pore space is clearly illustrated by the resistivity of the chalk sample N-3X 17V during the injection with deionized water, after 60 PVI. In spite of the highly resistive injected water, the resistivity of the core remained below 100 Ohm m.

4.3.2. Greensand from Solsort field

Core plugs D03H, D04H, D07H and D17H were flooded at 39 MPa axial and 40 MPa radial stresses at 60 °C. Fig. 15 shows the pore compressibility of greensand during flooding and the oil recovery curve,

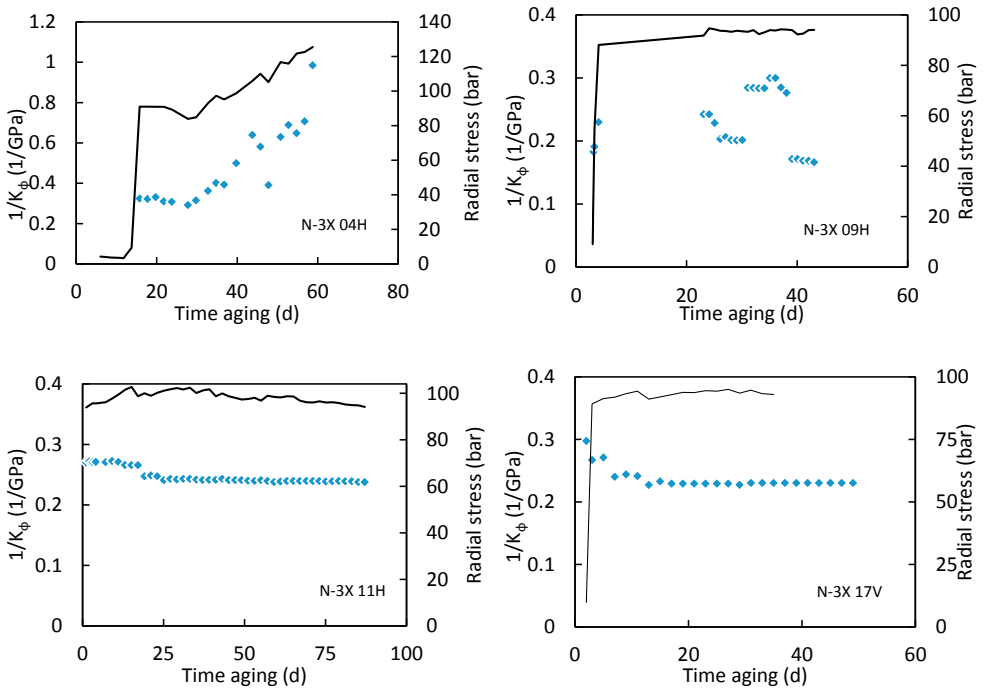

Fig. 9. The pore compressibility (1/Kϕ, diamond symbols) of the oil and water saturated chalk samples from the Gorm field at irreducible water saturation during aging at 60 °C (N-3X 04H, N-3X 09H, N-3X 11H, and N-3X 17V). The radial confining stress is shown for reference. The missing sequential data are due to experimental malfunctions.

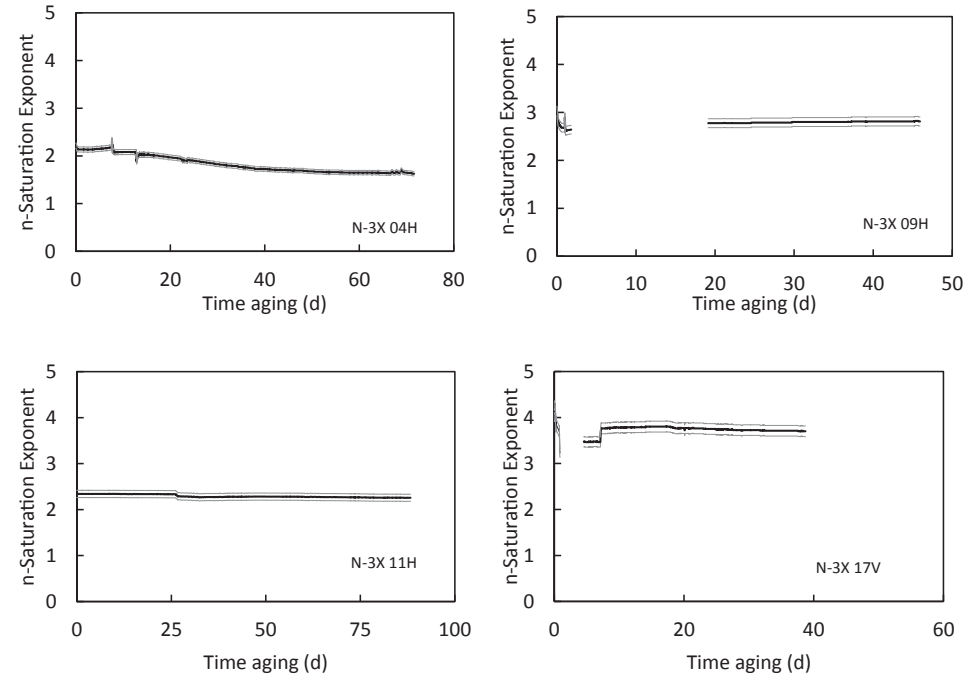

Fig. 10. The n-exponent of the oil and water saturated chalk samples from the Gorm field at irreducible water saturation during aging at 60 °C (N-3X 04H, N-3X 09H, N-3X 11H, and N-3X 17V). The missing sequential data are due to experimental malfunctions.

and Fig. 16 shows the resistivity of the injected bine, the resistivity of the brine present in the pore space during water flooding as well as the resistivity of the core plug at the same conditions.

During aging and flooding of the greensand samples D03H, D07H, D04H and D17H, the pore compressibility varies between 0.1 GPa^{-1} and 0.3 GPa^{-1} (Figs. 11 and 15). The pore compressibility of greensand seems to be unaffected by the presence of various ions in the pore space, possibly because the frame stiffness is determined by the quartz rather than the more surface active clay minerals.

During flooding of the greensand samples, the resistivity of the pore water was found to be higher than the resistivity of the injected brine indicating that the formation brine is not fully replaced during flooding. This is illustrated by the resistivity of the greensand samples D04H and D07H during the injection with low salinity brine and deionized water.

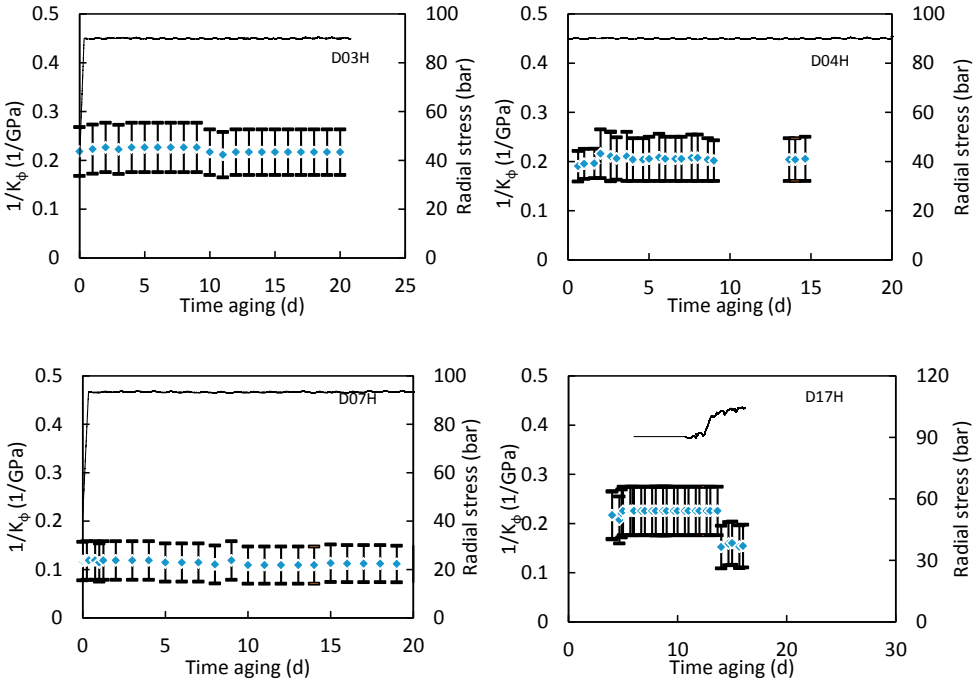

Fig. 11. The pore compressibility (1/Kϕ, diamond symbols) of the oil and water saturated greensand samples from the Solsort field at irreducible water saturation during aging at 60 °C (D03H, D04H, D07H, and D17H). Confining stress is shown for reference. The missing sequential data are due to experimental malfunctions. The error bars define the wide range of the bulk modulus of the rock mineral mixture.

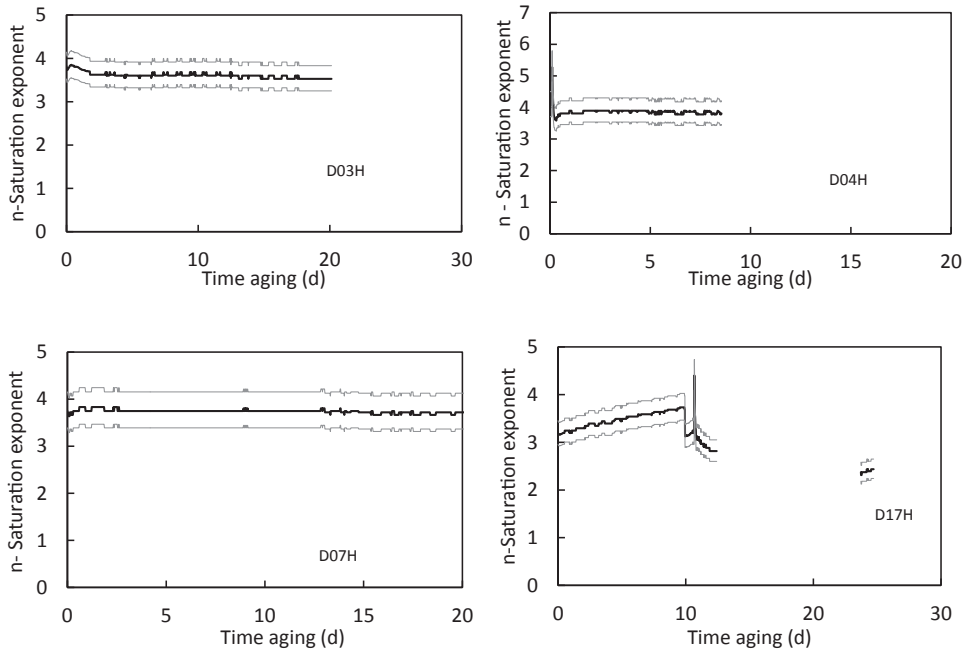

Fig. 12. The n-exponent of the oil and water saturated greensand samples from the Solsort field at irreducible water saturation during aging at 60 °C, (D03H, D04H, D07H, and D17H). The missing sequential data are due to experimental malfunctions.

The expected resistivity of the core should have been above 1000 Ohm m, whereas the resistivity of the core was found to be below 100 Ohm m (Fig. 16).

4.4. Petrophysical investigation after flooding

After flooding, all samples were cleaned using the Soxhlet method and afterwards dried for 3 days at 60 °C. Then, porosity, permeability and BET specific surface were measured and shown in Table 14. The specific surface of chalk increased after aging and flooding indicating the possible precipitation of fines. After flooding, chalk samples N-3X 04H and N-3X 11H, demonstrate a water NMR peak approximately at 100 ms, similar to the water peak of the water saturated chalk sample N-3X X02H, indicating full water wetness after flooding (Figs. 4, 5). Some remaining

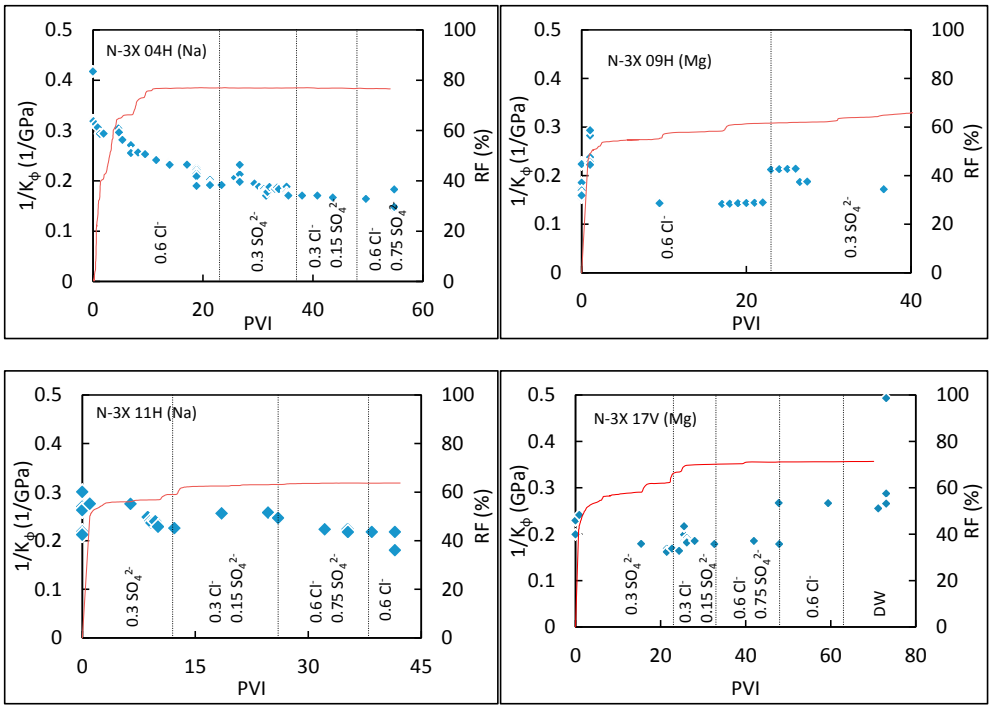

Fig. 13. The pore compressibility (1/Kϕ) from ultrasonic data, of the oil and water saturated chalk samples from the Gorm field as function of pore volumes injected (PVI) at 60 °C (N-3X 04H, N-3X 09H, N-3X 11H, and N-3X 17V). The missing sequential data are due to experimental malfunctions. Recovery factor (RF) is shown by continuous line. Differential pressure (DP) between inlet and outlet: for sample N-3X 04H DP was constant equal to 7 bar; for sample N-3X 09H DP decreased gradually from 2 bar to 1 bar during the first 10 pore volumes and was 1 bar during the remaining experiment; for sample N-3X 11H DP decreased gradually from 4 bar to 2.5 bar during the first 8 pore volumes and was 2.5 bar during the remaining experiment; for sample N-3X 17V DP was equal to 20 bar for the first 15 pore volumes, then dropped to 5 bar and gradually rose to 18 bar at 21 pore volumes, for the remaining test DP was equal to 8 bar.

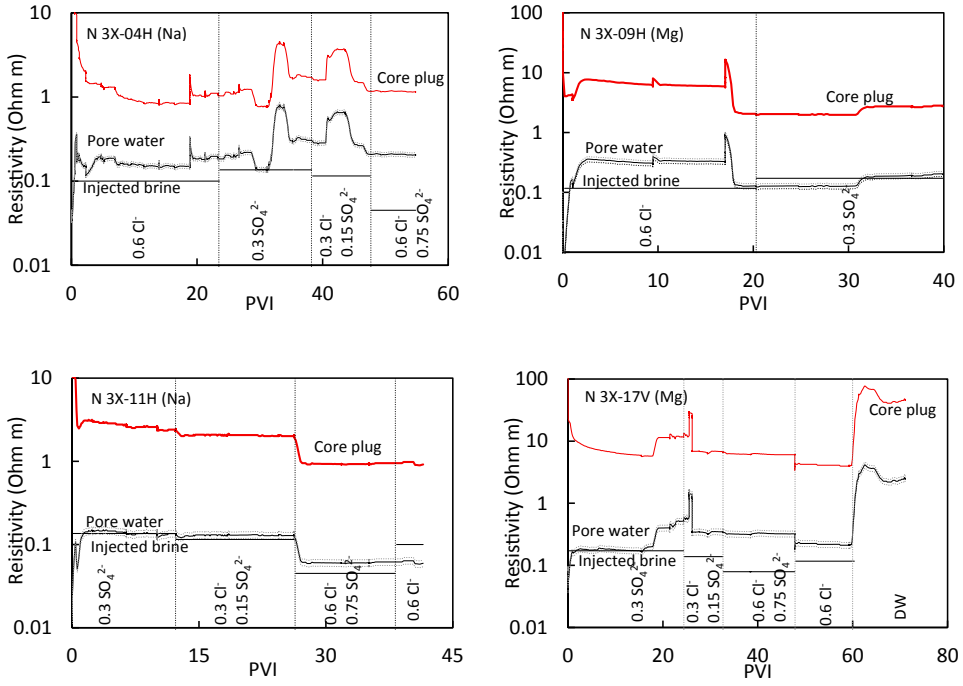

Fig. 14. The resistivity of the injected bine and the resistivity of the brine present in the pore space, as well as the resistivity of the core plug during water flooding of the oil and water saturated chalk samples from the Gorm field (N-3X 04H, N-3X 09H, N-3X 11H, and N-3X 17V).

peaks in Fig. 5 could be attributed to the presence of oil in the pore space. The throat size distribution from MICP is shifted slightly to lower diameters (Fig. 3). This might be caused by fines in the pore space, but the shift in MICP is small and NMR did not indicate the presence of fines.

Neither MICP nor the specific surface of greensand samples demonstrate significant changes during aging and flooding (Fig. 3, Tables 10, 14), but NMR data show a shift to lower relaxation times in the slow relaxing components in the T_2 distributions after flooding for D04H,

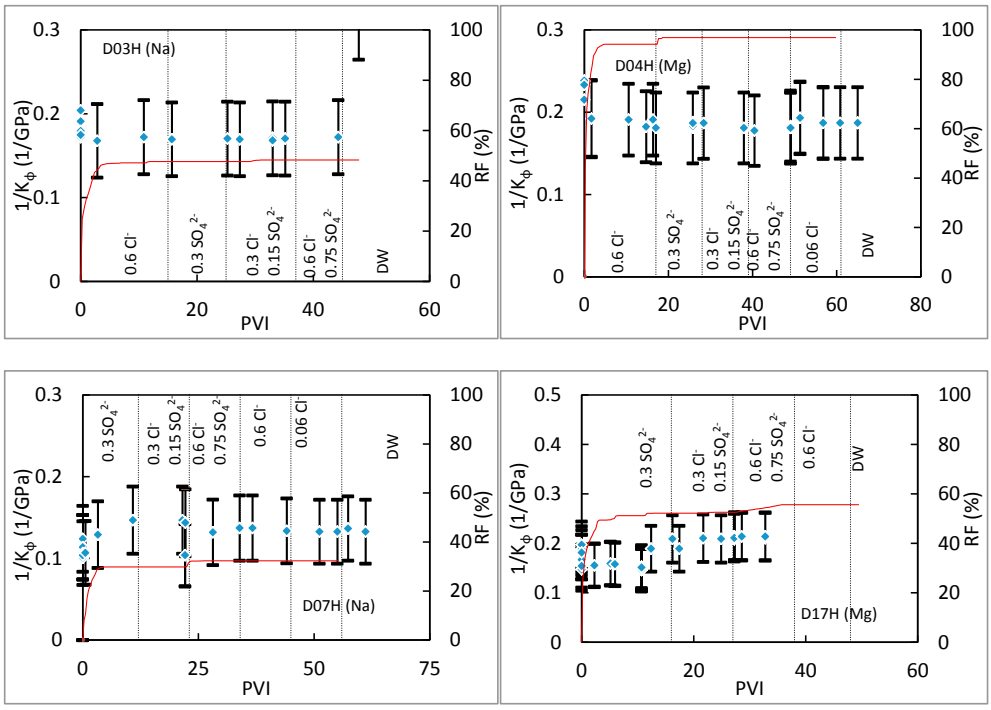

Fig. 15. The pore compressibility (1/Kϕ) from ultrasonic data, of the oil and water saturated greensand samples from the Solsort field during water flooding at 60 °C, (D03H, D04H, D07H, and D17H). PVI is pore volumes injected. The error bars define the wide range of the bulk modulus of the rock mineral mixture. Recovery factor (RF) is shown by continuous line. Differential pressure (DP) between inlet and outlet: for sample D0H3 DP varied between 0.3 bar (beginning of new fluid) and 0.6 (end of fluid) throughout the test; for sample D0H4 DP was constant equal to 3 bar; for sample D07H DP was constant equal to 2 bar; for sample D17H DP was constant equal to 1 bar for the first 5 pore volumes, for the remaining test it was constant equal to 3 bar.

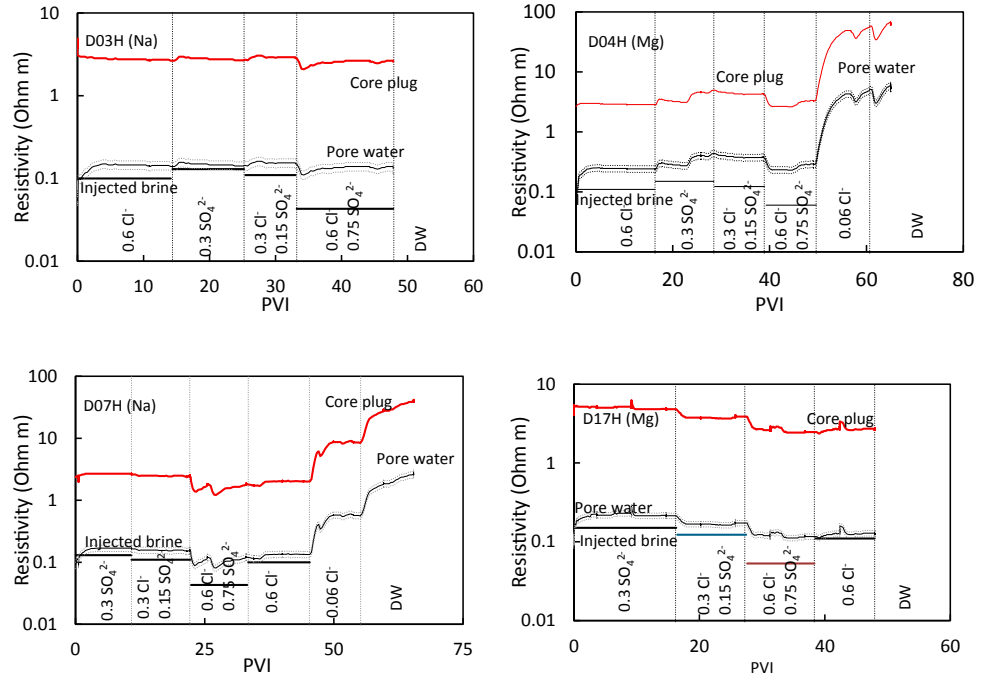

Fig. 16. The resistivity of the injected brine and the resistivity of the brine present in the pore space, as well as the resistivity of the core plug during water flooding of the oil and water saturated greensand samples from the Solsort field during water flooding, (D03H, D04H, D07H, and D17H).

D07H, and D17H (Fig. 8). This is probably due to the slow bulk relaxation of the oil that does not contact the surface of the quartz grains at S_{wir}. After flooding the slow relaxing oil is displaced by water that relaxes faster in contact with the surface of quartz (Katika et al., 2016). It is as yet unexplained why the slow relaxing peak of the sample D03H does not shift to faster relaxation upon flooding (Fig. 8).

Table 14
Petrophysical properties of aged and water flooded chalk and greensand samples (after Soxhlet extraction, cleaning and drying at 60 °C).

Sample ID	Porosity (%)	Permeability (mD)	BET (m^2/g)
Error	±0.3	±0.1	±0.03
D07H	34	106	7.5
D17H	35	65	7.1
N-3X 09H	35	0.9	2.0

5. Discussion

5.1. Wettability alteration

A wettability change from water wet to less water wet was indicated by NMR data collected before and after aging of one chalk sample (N-3X X02H). We assume that before aging of the chalk sample, the fast relaxing components correspond to the relaxation of the water bound to the surface and the slow relaxing components correspond to the relaxation of the bulk oil according to previous studies of rocks saturated with two fluids (Guan et al., 2002; Katika et al., 2016). After aging, the relaxation of the bulk oil is faster, indicating that the pore fluid distribution in the chalk has changed and that the oil partly wets the surface of the minerals (Al-Mahrooqi et al., 2003). Changes in the wettability of chalk after aging could be due to the saturation procedure (evaporation method) that resulted in a thin layer of water at irreducible water saturation. A thin water layer may be sensitive to evaporation due to the high temperature applied to the core during aging, so that water vapour enters the oil phase and oil components enter the water phase. One sample obtained an electrical n-exponent higher than 3 during aging as an indication of intermediate wetness (Sweeney and Jennings, 1960; Suman and Knight, 1997), whereas three samples retained an n-exponent between 2 and 3 indicating that they remained water-wet during aging. Upon flooding, NMR data indicate that all chalk samples were water-wet. As indicated by NMR data, all greensand samples remained mixed wet from before to after flooding. These results would indicate that at 60 °C an enhanced oil recovery mechanism due to wettability change is unlikely in the studied greensand and chalk. This negative result from chalk is in marked contrast to results from earlier studies where a wettability change was inferred to be a major cause of enhanced oil recovery in chalk (e.g. Austad et al., 2008). It should be noted that these earlier studies addressed chalk at high temperature (90 °C-130 °C) corresponding to the deeper location of the Norwegian chalk fields as compared to the studied Danish chalk field. In this context it is relevant that chalk would tend to be more oil wet at higher temperatures.

5.2. Pore compressibility

The ultimate oil recovery of the Na-flooded chalk is achieved before 15 pore volumes are injected in the core, whereas, more than 20 pore volumes have to be injected in the Mg-flooded rocks to stabilize the oil recovery factor (Fig. 13). During water flooding, the initial formation brine and oil are partly pushed out of the rock due to the injection of water with selective ions. We propose the following mechanism: Before water flooding, Na^+ and Ca^{2+} from the pore water is adsorbed on the calcite surface, but upon flooding with Na^+ brine, adsorbed Ca^{2+} is fully or partly replaced by Na^+. This causes the charge of the calcite crystals to fall and the internal repulsive force to diminish and the chalk to stiffen, conversely, when Na^+ is replaced by Mg^{2+}, the surface charge increases and the chalk softens. Replacing the Ca^{2+} of the formation brine with Na^+ is a fast procedure that makes the rock stiffer, whereas, replacement of Na^+ and Ca^{2+} with Mg^{2+}, results in chalk softness after the injections of more pore volumes.

Consequently, the overall pore compressibility of chalk decreases during flooding with Na-rich brines and increases during flooding with Mg-rich brines (Fig. 13). This is in accordance with previous findings on chalk from Stevns Klint, where chalk saturated with Mg-rich brines is mechanically softer than chalk saturated with Na-rich brines (Katika et al., 2015). In other chalks, NaCl brines resulted in lower disjoining forces between the grains of chalk than Na_2SO_4 brines; therefore, the bulk modulus of chloride bearing chalk is higher (and pore compressibility lower) than the sulphate saturated chalk (Nermoen et al., 2015).

During flooding with water containing softening ions, as Mg^{2+}, an increased pore compressibility will cause the pressure in the reservoir fluids to increase in the flooded area leading to enhanced oil recovery.

The pore compressibility of the greensand samples does not demonstrate a trend during water flooding with selective ions (Fig. 15). Overall, samples that have low final oil recovery have low pore compressibility. Greensand is relatively stiff when water is occupying the pore space of the rock because of the stiffer water than oil.

These results would indicate that at 60 °C changes in pore compressibility is a viable enhanced oil recovery mechanism in chalk due to change in charge of the adsorbed ions on the calcite surface. The mechanism is unlikely in the studied greensand.

5.3. Fines formation

According to Katika et al. (2015), the formation of fines and precipitation reactions alter the surface to volume ratio of the rock and cause shifts in the T_2 distribution, a shift of this type was not observed by NMR, but a small shift to lower values was found from MICP and an increase in BET was observed. This would indicate that we cannot exclude a mechanism involving the precipitation of fines in the chalk pores during flooding in accordance with the prediction of Chakravarty et al. (2015). The studied very pure chalk contains only little natural fines, so a fines mobilization mechanism can probably be disregarded. No indication of fines formation or fines mobilization was found for the greensand samples.

6. Conclusions

Four chalk samples from the Gorm field and four greensand samples from the Solsort field, both in the North Sea, were aged and flooded at 60 °C. Low field NMR spectrometry, elastic waves and electrical resistivity were the main tools used to define the mechanisms related to changes in petrophysical and mechanical properties of the rocks during water flooding.

- Electrical resistivity data and NMR indicate that chalk is water wet upon saturation to S_{wir}, but that aging in some cases leads to a wettability change to less water wet conditions (this can be a consequence of the evaporation method used for saturation). Upon flooding all chalk samples regained their water wetness.
- Electrical resistivity and NMR data indicate that greensand remains mixed wet during aging and flooding.
- According to the ultrasonic velocities, flooding of chalk with Mg-bearing brines results in lower pore compressibility of chalk than flooding with Na-rich brines (mechanical weakening).
- Pore water composition was not seen to affect the pore compressibility of greensand.
- Fines formation caused by chemical precipitation during flooding of chalk may be inferred from increase specific surface and a small shift to lower average throat diameter by MICP, although no shift in the NMR curve was observed. No fines formation was indicated in greensand.
- In summary: at 60 °C no oil production effect of flooding with selective ions was found in the studied greensand. For the studied chalk, no effect of wettability change was documented; whereas an effect of fines formation cannot be excluded, and an effect due to changing pore compressibility may have most significance.

Acknowledgments

The authors thank the Danish Energy Agency EUDP 10-II Grant 64011-0009, Mærsk Oil and DONG Energy for funding. We thank Alexander Shapiro and Kaj Thomsen for fruitful discussions. We also thank two anonymous reviewers for constructive comments.

References

Al-Mahrooqi, S., Grattoni, C.A., Moss, A.K., Jing, X.D., 2003. An investigation of the effect of wettability on NMR characteristics of sandstone rock and fluid systems. Petrol. Sci. Eng. 39, 389–398.

American Petroleum Institute, 1998. e In: Recommended Practices for Core Analysis, Recommended Practic, 2.nd ed., vol. 40. API Publications and Distribution, pp. 682–8375. (202).

Andersen, P.Ø., Evje, S., Madland, M.V., Hiorth, A., 2012. A geochemical model for interpretation of chalk core flooding experiments. Chem. Eng. Sci. 84, 218–241.

Archie, G.E., 1942. The electrical resistivity log as an aid in determining some reservoir characteristics. Pet. Trans. AIME 146 (8), 54, 52.

Austad, T., Strand, S., Høgnesen, E.J., Zhang, P., 2005. Seawater as IOR fluid in fractured chalk. In: SPE International Symposium on Oilfield Chemistry. Society of Petroleum Engineers Inc., The Woodlands, Texas.

Austad, T., Strand, S., Madland, M.V., Puntervold, T., Korsnes, R.I., 2008. Seawater in chalk: an EOR and compaction fluid. SPE Reserv. Eval. Eng. 11 (4), 648–654.

Batzle, M.L., Wang, Z., 1992. Seismic properties of pore fluids. Geophysics 57, 1396–1408.

Brunauer, S., Emmett, P.H., Teller, E., 1938. Adsorption of gases in multimolecular layers. Am. Chem. Soc. 60 (2), 309–319.

Bæk, M., 2014. Oil and Gas Production in Denmark and Subsoil Use. Danish Energy Agency. ISBN: www-978-87-93071-71-1, ISSN: 1904-0253.

Chakravarty, K.H., Fosbøl, P.L., Thomsen, K., 2015. Fine formation during brine-crude oil-calcite interaction in smart water enhanced oil recovery for caspian carbonates. In: Proceedings of the SPE Annual Caspian Technical Conference & Exhibition. Society of Petroleum Engineers. SPE-177379-MS.

Fabricius, I.L., 2007. Chalk: composition, diagenesis and physical properties. Bull. Geol. Soc. Den. 55, 97–128.

Fathi, S.J., Austad, T., Strand, S., 2010. 'Smart water' as a wettability modifier in chalk: the effect of salinity and ionic composition. Energy & fuels 24, 2514–2519.

Gassmann, F., 1951. Uber die Elastizitaet poroeser Medien: vierteljahresschrift der Naturforschenden Gesellschaft. Zuerich 96, 1–23.

Guan, H., Brougham, D., Sorbie, K.S., Packer, K.J., 2002. Wettability effects in a sandstone reservoir and outcrop cores from NMR relaxation time distributions. Petrol. Sci. Eng. 34, 35–54.

Hiorth, A., Cathles, L., Madland, M., 2010. The impact of pore water chemistry on carbonate surface charge and oil wettability. Transp. Porous Media 85 (1), 1–21.

Hürlimann, Mand.D., Matteson, A., Massey, J.E., Allen, D.F., Fordham, E.J., Antonsen, F., Rueslåtten, H.G., 2004. Application of NMR diffusion editing as chlorite indicator. Petrophysics 45 (5), 414–421.

Jackson, M.D., Vinogradov, J., Hamon, G., Chamerois, M., 2016. Evidence, mechanisms and improved understanding of controlled salinity waterflooding part 1: Sandstones. Fuel 185, 772–793.

Jadhunandan, P.P., Morrow, N.R., 1995. Effect of wettability on waterflood recovery for crude-oil/brine/rock systems. SPE Reserv. Eng. 10 (1), 40–46.

Katika, K., Addassi, M., Alam, M.M., Fabricius, I.L., 2015. The effect of divalent ions on the elasticity and pore collapse of chalk evaluated from compressional wave velocity and low-field Nuclear Magnetic Resonance (NMR). Petrol. Sci. Eng. 136, 88–99.

Katika, K., Ahkami, M., Fosbøl, P.L., Halim, A.Y., Shapiro, A., Thomsen, K., Xiarchos, I., Fabricius, I.L., 2016. Comparative analysis of experimental methods for quantification of small amounts of oil in water. Petrol. Sci. Eng. 147, 459–467.

Katika, K., Saidian, M., Prasad, M., Fabricius, I.L., 2017. Low field NMR spectrometry of chalk and argillaceous sandstones: rock - fluid affinity assessed from T_1/T_2 ratio. Petrophysics 58, 126–140.

Korsnes, R.I., Strand, S., Hoff, O., Pedersen, T., Madland, M.V., Austad, T., 2006. Does the chemical interaction between seawater and chalk affect the mechanical properties of chalk. EUROCK 2006, 427–434.

Madland, M.V., Hiorth, A., Omdal, E., Megawati, M., Hildebrand-Habel, T., Korsnes, I.R., Evje, S., Cathles, M.L., 2011. Chemical alterations induced by rock-fluid interactions when injecting brines in high porosity chalks. Transp. Porous Med. 87, 679–702.

Mavko, G., Mukerji, T., Dvorkin, J., 2009. The Rock Physics Handbook: Tools for Seismic Analysis of Porous Media, second ed. Cambridge University Press. ISBN 9780521861366.

Morrow, N.R., Tang, G.-Q., Valat, M., Xie, X., 1998. Prospects of improved oil recovery related to wettability and brine composition. Petrol. Sci. Eng. 20 (3–4), 267–276.

Nermoen, A., Korsnes, R.I., Fabricius, I.L., Madland, M.M., 2015. Extending the effective stress relation to incorporate electrostatic effects. In: SEG New Orleans Annual Meeting 2015, pp. 3239–3243.

Newman, G.H., 1983. The effect of water chemistry on the laboratory compression and permeability characteristics of some North Sea chalks. J. Pet. Tech. 35, 976–980.

Puntervold, T., Austad, T., 2008. Injection of seawater and mixtures with produced water into North Sea chalk formation: impact on wettability, scale formation and rock mechanics caused by fluid-rock interaction. J. Petrol. Sci. Eng. 63 (1–4), 23–33.

Radke, C.J., Kovscek, A.R., Wong, H., 1992. A Pore-Level Scenario for the Development of Mixed Wettability in Oil Reservoirs. SPE-24880-MS.

Revil, A., 2013a. Effective conductivity and permittivity of unsaturated porous materials in the frequency range 1 mHz–1GHz. Water Resour. Res. 49, 306–327.

Revil, A., 2013b. On charge accumulation in heterogeneous porous rocks under the influence of an external electric field. Geophysics 78, D271–D291.

Schlumberger Wireline & Testing, 2000. Log Interpretation Charts. Gen 7–9.

Seccombe, C.J., Lager, A., Webb, K., Jerauld, G., Fueng, E., 2008. Improving waterflood recovery: LoSalTM EOR field evaluation. In: SPE/DOE Imp. Oil Rec. Symposium. Tulsa, Oklahoma.

Strand, S., Høgnesen, E.J., Austad, T., 2006. Wettability alteration of carbonates-Effects of potential determining ions (Ca2+ and SO42-) and temperature. Colloids Surfaces A Physicochem. Eng. Aspects 275 (1–3), 1–10.

Suman, R.J., Knight, R.J., 1997. Effects of pore structure and wettability on the electrical resistivity of partially saturated rocks; a network study. Geophysics 62 (4), 1151–1162.

Sweeney, S., Jennings, J.R.,H., 1960. Effect of wettability on the electrical resistivity of carbonate rock from a petroleum reservoir. J. Phys. Chem. 64, 551–553.

Vledder, P., Fonseca, J.C., Wells, T., Gonzalez, I., Ligthelm, D., 2010. Low Salinity Water Flooding: Proof of Wettability Alteration on a Field Scale. SPE 129564.

Wang, Z., Wang, H.F., Cates, M., 2001. Effective elastic properties of solid clays. Geophysics 66, 428–440.

Yousef, A.A., Al-Saleh, S.H., Al-Kaabi, A., Al-Jawfi, M.S., 2011. Laboratory investigation of the impact of injection-water salinity and ionic content on oil recovery from carbonate reservoirs. SPE Reserv. Eval. Eng. 14 (5), 578–593.

Yutkin, M., Lee, J.Y., Mishra, H., Radke, C.J., Patzek, T.W., 2016. Bulk and surface aqueous speciation of calcite: implications for low-salinity waterflooding of carbonate reservoirs. SPE-182829-MS. In: SPE Kingdom of Saudi Arabia Annual Technical Symposium and Exhibition, Damman, Saudi Arabia 26-28 April, 2016, 29 pp.

Zhang, P., Tweheyo, M.T., Austad, T., 2007. Wettability alteration and improved oil recovery by spontaneous imbibition of seawater into chalk: impact of the potential determining ions Ca^{2+}, Mg^{2+}, and SO_4^{2-}. Colloids Surf. A Physicochem. Eng. Asp. 301, 199–208.